

Relativistic Three-Quark Bound States in Separable Two-Quark Approximation

M. Oettel ^a, L. von Smekal ^b, R. Alkofer ^c

^a*CSSM, University of Adelaide, 10 Pulteney St., Adelaide, SA 5005,
E-mail: moettel@physics.adelaide.edu.au*

^b*Institut für Theoretische Physik III, Universität Erlangen–Nürnberg, Staudtstr. 7,
91058 Erlangen, Germany, E-mail: smekal@theorie3.physik.uni-erlangen.de*

^c*Institut für Theoretische Physik, Universität Tübingen, Auf der Morgenstelle 14,
72076 Tübingen, Germany, E-mail: Reinhard.Alkofer@uni-tuebingen.de*

Abstract

Baryons as relativistic bound states in 3-quark correlations are described by an effective Bethe-Salpeter equation when irreducible 3-quark interactions are neglected and separable 2-quark correlations are assumed. We present an efficient numerical method to calculate the nucleon mass and its covariant wave function in this quantum field theoretic quark-diquark model with quark-exchange interaction. Expanding the components of the spinorial wave function in terms of Chebyshev polynomials, the four-dimensional integral equations are in a first step reduced to a coupled set of one-dimensional ones. This set of linear and homogeneous equations defines a generalised eigenvalue problem. Representing the eigenvector corresponding to the largest eigenvalue, the Chebyshev moments are then obtained by iteration. The nucleon mass is implicitly determined by the eigenvalue, and its covariant wave function is reconstructed from the moments within the Chebyshev approximation.

PACS Numbers: 02.30.Rz, 11.10.St, 12.39.Ki, 12.40.Yx

PROGRAM SUMMARY

Title of program: BSE

Computers: Workstation DEC Alpha, LINUX PCs (AMD K7)

Operating system under which the program has been tested: UNIX, Linux

Programming language used: Fortran 90

Memory required to execute with typical data: 10 MB

No. of bits in a word: 32

Peripherals used: standard output, disk

No. of lines in distributed program, including test data, etc.:

Keywords: linear integral equations; Bethe–Salpeter equation; nucleon model; diquarks.

Nature of physical problem: Diquarks are introduced as separable correlations in the two-quark Green’s function to facilitate the description of baryons as relativistic three-quark bound states. These states then emerge as solutions of Bethe–Salpeter equations for quarks and diquarks that interact via quark exchange.

Method of solution: Chebyshev polynomials are used for an expansion of the Bethe–Salpeter vertex and wave functions and an (approximative) representation of the interaction kernel and propagators. The resulting set of coupled one-dimensional integral equations for the corresponding moments of vertex and wave function is converted to a matrix equation by employing Gaussian quadrature grid points. This equation is then solved iteratively for a certain test mass of the bound state. A bisection method in the bound state mass variable is used to determine the correct mass corresponding to the chosen quark and diquark parameters.

Restrictions on the complexity of the problem: The separable quark-quark correlations are restricted to the leading covariants in the scalar and axialvector (i.e. positive parity) channels.

Typical running time: Depending on the parameters and the desired accuracy between one and ten minutes on 1.2 GHz AMD K7.

LONG WRITE-UP

1 The physical problem

A Poincaré-invariant, quantum field theory based model of the nucleon is required to describe the high-precision data of nucleon properties in the several-GeV energy range. To this end, we here demonstrate how to calculate (using certain approximations detailed below) the matrix elements of three quark operators q between the vacuum $|\Omega\rangle$ and the nucleon bound state $|P_N\rangle$, the asymptotic momentum state with nucleon quantum numbers. This matrix element $\psi \sim \langle\Omega|T(qqq)|P_N\rangle$ is the covariant Bethe–Salpeter wave function of the nucleon which can be applied as input in covariant calculations of many observables such as the various form factors of the nucleon. In the following sections we describe an approximation scheme based on the Faddeev equations (see, *e.g.*, ref. [1]) which makes use of the concept of diquarks as separable quark-quark correlations [2–8]. In this scheme, the covariant diquark-quark model, see refs. [9–16], we obtain a tractable set of equations for the components of the covariant nucleon wave function which can be solved without non-relativistic reductions.

1.1 The separable approximation to the relativistic 3-quark problem

To summarize the relation between the covariant quark-diquark model and the general, relativistic three-quark problem briefly in the following, we start from the six-quark Green function,

$$G(x_i, y_i) = \langle 0|T \prod_{i=1}^3 q(x_i)\bar{q}(y_i)|0\rangle. \quad (1)$$

The variables x_i and y_i not only represent the space-time coordinates of the quark fields, but also include their discrete labels for color, spin, and flavor. The six-point function (1) satisfies the Dyson equation

$$G = G_0 + G_0 \circ K \circ G. \quad (2)$$

In this equation the disconnected six-point function G_0 describes the free propagation of three dressed quarks, and the three-quark scattering kernel K contains all two- and three-particle irreducible diagrams. The symbol “ \circ ” in eq. (2) denotes summation/integration over all independent internal coordinates and labels which defines a composition law for linear maps on a suitable function space. Unless explicitly stated otherwise we will henceforth work in

momentum space with Euclidean metric. It is thus not necessary to introduce different symbols for momentum and coordinate space objects.

The nucleon as a three-particle bound state with mass M manifests itself as a pole in the six-point function at $-P^2 = M^2$ where $P = p_1 + p_2 + p_3$ is the total four-momentum of the three-quark system. One can thus parameterize the six-point function in the vicinity of the pole as

$$G(k_i, p_i) \sim \frac{\psi(k_1, k_2, k_3) \bar{\psi}(p_1, p_2, p_3)}{P^2 + M^2}, \quad (3)$$

where ψ denotes the bound state wave-function. Substituting this parameterization into the Dyson equation (2) and identifying the residuum contributions on both sides, one obtains the homogeneous bound state equation,

$$\psi = G_0 \circ K \circ \psi \quad \iff \quad G^{-1} \circ \psi = 0. \quad (4)$$

Despite the simple appearance of the bound state equation in this symbolic form, its direct solution is not feasible. Even in principle, this could only be attempted once a model interaction is specified to fix the contributions to the kernel K which can in general never be fully determined from first principles.

The approximation scheme we present below essentially consists of two steps. Thereby, some of the contributions to the kernel, namely those due to irreducible three-particle interactions, are neglected while an explicit reference to the others is avoided by shifting the details of the two-particle interactions into the parametrisations of the relevant diquark correlations.

The first step leads to the corresponding relativistic Faddeev equations. Neglecting all contributions from irreducible three-quark interactions, the kernel K can be written as a sum of three two-quark interaction kernels,

$$K = K_1 + K_2 + K_3. \quad (5)$$

We adopt the notation that the subscript of K_i refers to the spectator quark q_i . The $K_i = k_{qq} \otimes S_i^{-1}$ are defined in 3-quark space and thus contain an inverse quark propagator S_i^{-1} acting on the subspace of the spectator quark. The quark pair interacting via k_{qq} in K_i then is (q_j, q_k) with the three labels (i, j, k) being a cyclic permutation of $(1, 2, 3)$. These 2-quark kernels determine the interactions for disconnected scattering amplitudes $T_i = t_{qq} \otimes S_i^{-1}$ which describe the scattering between quark j and k (with amplitude t_{qq}) and which are summed in the Dyson series for this 2-quark subspace as follows:

$$T_i = K_i + K_i \circ G_0 \circ T_i. \quad (6)$$

Introducing the Faddeev components of the 3-quark wave function ψ ,

$$\psi_i = G_0 \circ K_i \circ \psi, \quad (7)$$

one then has $\psi = \sum \psi_i$ by virtue of eqs. (4,5). Furthermore, eq. (6) can now be used to simplify eq. (4) considerably yielding the coupled Faddeev equations,

$$\psi_i = G_0 \circ T_i \circ (\psi_j + \psi_k) , \quad (8)$$

for Faddeev components with pairwise distinct $i, j, k \in \{1, 2, 3\}$.

The assumption central to the second step, and the defining one of the quark-diquark model, is the *separability* of the two-quark scattering amplitude t_{qq} . This amplitude is thereby typically parametrised by *scalar* and *axialvector* diquark correlations to account for its most important separable contributions at sufficiently small (absolute values of the complex Euclidean) diquark momenta,

$$t_{qq}(k_j, k_k; p_j, p_k) = \chi^5((k_j - k_k)/2) D^{55}(k_j + k_k) \bar{\chi}^5((p_j - p_k)/2) + \chi^\mu((k_j - k_k)/2) D^{\mu\nu}(k_j + k_k) \bar{\chi}^\nu((p_j - p_k)/2) . \quad (9)$$

Here we employ simple particle-pole contributions to represent these diquark correlations. The diquark propagators are then given by the free scalar propagator and the Proca propagator for a spin-1 particle, respectively,

$$D^{55}(p) = -\frac{1}{p^2 + m_{sc}^2} , \quad (10)$$

$$D^{\mu\nu}(p) = -\frac{1}{p^2 + m_{ax}^2} \left(\delta^{\mu\nu} + \frac{p^\mu p^\nu}{m_{ax}^2} \right) . \quad (11)$$

The diquark-quark vertices χ in eq. (9) need to be antisymmetric with respect to the interchange of their quark indices. Both diquarks belong to the antisymmetric color antitriplet. The scalar diquark vertex is an antisymmetric isospin singlet and is also antisymmetric in Dirac space while the axialvector diquark vertex is symmetric in both Dirac and isospin indices (triplet). We do not give their color and flavor structures explicitly here, and we restrict the Dirac structures of both χ to the dominant ones which are given by

$$\chi_{jk}^5(p) = g_s (\gamma^5 C)_{jk} V_s(p) , \quad (12)$$

$$\chi_{jk}^\mu(p) = g_a (\gamma^\mu C)_{jk} V_a(p) , \quad (13)$$

respectively, where g_s and g_a represent coupling constants which are determined by the diquark normalizations, see below. The scalar functions $V_{s,a}(p)$ parametrise the extensions of the two diquark-quark amplitudes in momentum space. Phenomenologically, a dipole form for their dependence on the quark relative momenta has proven successful, and we will assume equal widths for

both diquarks here,

$$V_s(p) = V_a(p) = \left(\frac{c_0^2}{c_0^2 + p^2} \right)^2, \quad (14)$$

to reveal the general structures in a reasonably simple form in the following.

The diquark widths determine their couplings g_s and g_a by normalization conditions derived from the Bethe-Salpeter equation (6) for the 2-quark scattering amplitude,

$$t_{qq} = k_{qq} + k_{qq} \circ (S \otimes S) \circ t_{qq}. \quad (15)$$

Inserting the ansatz (9) with the diquark pole contributions (10,11) into in the inhomogeneous equation (15) implicitly fixes the normalizations adopted for the diquark amplitudes. These implicit conditions are most easily derived from the derivative of eq. (15) w.r.t. the total diquark momentum $P_d = k_j + k_k$, for details, see *e.g.* refs. [9,14]. Under the mild additional assumption that the 2-quark interaction kernel k_{qq} be independent of P_d , the normalization conditions for the scalar and axialvector diquark amplitudes are,

$$4 m_{sc}^2 \stackrel{!}{=} \bar{\chi}^5 \circ \left(P_d \cdot \frac{\partial}{\partial P_d} (S \otimes S) \right) \circ \chi^5, \quad (16)$$

$$12 m_{ax}^2 \stackrel{!}{=} \bar{\chi}^\nu \circ \left(P_d \cdot \frac{\partial}{\partial P_d} (S \otimes S) \right) \circ \chi^\mu \left(\delta^{\mu\nu} + \frac{P_d^\mu P_d^\nu}{m_{ax}^2} \right), \quad (17)$$

respectively. The additional factor of 3 in the last line arises from the sum over the polarisation states of the spin-1 particle.

1.2 The quark-diquark Bethe-Salpeter equation

For identical particles, the three Faddeev components (7) are obtained from a unique amplitude ϕ_{ijk} by cyclic permutations of the indices and arguments labelling the individual quarks, and the 3-quark amplitude is obtained by their sum or, equivalently, their Faddeev wave function by $\psi = G_0 \circ \sum_{cyclic} \phi_{ijk}$. With the separable form for the two-quark scattering amplitude t_{qq} in eq. (9), the following *ansatz* is employed in the Faddeev equations (8):

$$\begin{aligned} \phi_{ijk}(p_i, p_j, p_k) = & \quad (18) \\ \chi_{jk}^a(q) D^{ab} \left((1-\eta)P - p \right) \left(\Phi^b(p, P) u(P) \right)_i, & \quad (\mathbf{a}, \mathbf{b} = 1 \dots 5). \end{aligned}$$

Herein, $u(P)$ is a positive-energy spinor for the nucleon state with momentum $P = p_i + p_j + p_k$, $p = (1-\eta)p_i - \eta(p_j + p_k)$ is the relative momentum between

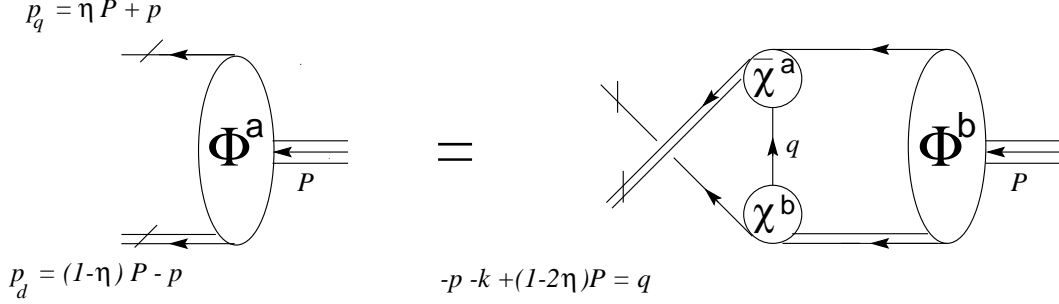


Fig. 1. The Bethe-Salpeter equation for the vertex function Φ .

quark and diquark, and $q = (p_j - p_k)/2$ is the relative momentum of the two quarks within the diquarks. We have introduced a momentum partitioning parameter $\eta \in [0, 1]$ which distributes the total momentum P between quark and diquark. An analogous parameter could also be introduced in a more general definition of the relative momentum q within the diquarks as discussed in [14]. Translational invariance entails that observables, *i.e.* matrix elements like the form factors etc., should not depend on such momentum partitioning parameters in the covariant bound-state wave functions. Furthermore, in eq. (18), Φ^a is composed of Dirac matrices such that $\Phi^{5[\mu]}u$ is the most general effective [vector] spinor compatible with nucleon quantum numbers for the Faddeev components. We call Φ^a the nucleon Bethe-Salpeter vertex function with quark and diquark.

The Faddeev equations (8) with the ansatz (18) now reduce to a system of effective 2-particle Bethe-Salpeter equations for a quark-diquark state bound by repeated quark-exchanges. Introducing an *eigenvalue* λ , for the lowest bound state in the given channel, these equations have to be solved for the largest value of $\lambda \equiv \lambda(P^2)$ at a given P^2 ,

$$\lambda(P^2) \Phi^a(p, P) = \int \frac{d^4k}{(2\pi)^4} K^{ab}(p, k, P) \Psi^b(k, P), \quad \text{with} \quad (19)$$

$$\Psi^a(p, P) = S(\eta P + p) D^{ab}((1-\eta)P - p) \Phi^b(p, P), \quad \text{and} \quad (20)$$

$$K^{ab}(p, k, P) = -\frac{1}{2} \begin{pmatrix} -\frac{1}{g_s^2} \chi^5(p_1) S^T(q) \bar{\chi}^5(p_2) & \frac{\sqrt{3}}{g_s^2} \chi^\beta(p_1) S^T(q) \bar{\chi}^5(p_2) \\ \frac{\sqrt{3}}{g_s^2} \chi^5(p_1) S^T(q) \bar{\chi}^\alpha(p_2) & \frac{1}{g_s^2} \chi^\beta(p_1) S^T(q) \bar{\chi}^\alpha(p_2) \end{pmatrix}, \quad (21)$$

with the additional constraint that $\lambda(P^2) = 1/g_s^2$ at $P^2 = M_n^2$, thereby implicitly determining the nucleon mass. We introduced the Bethe-Salpeter wave function $\Psi = G_0 \circ \Phi$ by attaching quark and diquark legs to the vertex function. With (20) in eq. (19) this determines a generalized eigenvalue problem in which the vertex function $\Phi = K \circ G_0 \circ \Phi$ represents an eigenvector of the kernel K with respect to a *metric* given by the disconnected quark-diquark

propagator,

$$G_0^{\text{ab}} = S(\eta P + p) D^{\text{ab}} ((1-\eta)P - p) (2\pi)^4 \delta^4(p - k) . \quad (22)$$

The numerical factors in the elements of the quark-exchange kernel K^{ab} arise from the structure of the color and flavor couplings in the Faddeev equations. Momentum conservation fixes the momentum of the exchanged quark,

$$q = -p - k + (1 - 2\eta)P , \quad (23)$$

and the relative momenta of the outgoing and the incoming quark-pair in $\chi(p_1)$ and $\bar{\chi}(p_2)$, respectively, are (see Fig. 1),

$$p_1 = p + k/2 - (1 - 3\eta)P/2 , \quad (24)$$

$$p_2 = -k - p/2 + (1 - 3\eta)P/2 . \quad (25)$$

Since neither the eigenvalue $\lambda = 1/g_s^2$ nor the mass M_n of the bound nucleon are allowed to depend on the momentum partitioning parameter η , for every solution $\Psi(p, P; \eta_1)$ of the Bethe-Salpeter equation (19) there should exist a whole family of solutions of the form $\Psi(p + (\eta_2 - \eta_1)P, P; \eta_2)$.

1.3 Decomposition of wave and vertex function

Having defined the effective spinor of the spectator quark to be $\Phi^{\text{a}}u$ in eq. (18) guarantees that the 3-quark wave function ψ describes a spin-1/2 object. Furthermore, Φ^{a} can most generally be chosen to be an eigenfunction of $\Lambda^+ = 1 + \hat{P}/(iM)$, the positive energy projector, since $\Lambda^-u = (1 - \Lambda^+)u = 0$. Requiring positive parity for the Faddeev amplitudes leads to the additional condition

$$\begin{pmatrix} \gamma^4 \Phi^5(\tilde{p}, \tilde{P}) \gamma^4 \\ \gamma^4 \tilde{\Phi}^\nu(\tilde{p}, \tilde{P}) \gamma^4 \end{pmatrix} \stackrel{!}{=} \begin{pmatrix} \Phi^5(p, P) \\ -\Phi^\nu(p, P) \end{pmatrix} , \quad (26)$$

with the parity operation on a 4-vector defined by $\tilde{q} = (-\vec{q}, q^4)^T$.

The positive-energy constraint and condition (26) greatly restrict the number of independent components in the vertex function. The scalar correlations Φ^5 are described by two components and the axialvector correlations by six components,

$$\begin{pmatrix} \Phi^5(p, P) \\ \Phi^\mu(p, P) \end{pmatrix} = \begin{pmatrix} \sum_{i=1}^2 S_i(p^2, \hat{p} \cdot \hat{P}) \mathcal{S}_i(p, P) \\ \sum_{i=1}^6 A_i(p^2, \hat{p} \cdot \hat{P}) \gamma_5 \mathcal{A}_i^\mu(p, P) \end{pmatrix} . \quad (27)$$

The scalar functions S_i and A_i depend on the two independent Lorentz invariants (p^2 and $p \cdot P$) that can be formed from the relative momentum p and the on-shell nucleon momentum P . Normalized 4-vectors are introduced as $\hat{p} = p/|p|$, and for the special case of the complex (*i.e.*, timelike) nucleon momentum we adopt the convention that $\hat{P} = P/(iM)$, see below.

The Dirac components describing the scalar correlations may be built out of Λ^+ and $\not{p}\Lambda^+$ and the Dirac part of the axialvector correlations can be constructed using the matrices $P^\mu\Lambda^+$, $P^\mu\not{p}\Lambda^+$, $\gamma^\mu\Lambda^+$, $\gamma^\mu\not{p}\Lambda^+$, $p^\mu\Lambda^+$ and $p^\mu\not{p}\Lambda^+$. Herein, for later convenience, we select a decomposition such that the scalar functions S_i and A_i decouple within the Dirac and Lorentz components of (27) in the nucleon rest-frame,

$$P = (\vec{0}, iM)^T, \quad (28)$$

and with additionally choosing the spatial part of the relative momentum to point in the z -direction (see sec. 2.1),

$$p = (0, 0, |p| \sin \psi, |p| \cos \psi)^T. \quad (29)$$

A decomposition of the covariants achieving this turns out to be given by

$$\mathcal{S}_i = \begin{cases} \mathcal{S}_1 = \Lambda^+ \\ \mathcal{S}_2 = -\frac{i}{p} \not{p}_T \Lambda^+ \end{cases}, \quad \mathcal{A}_i^\mu = \begin{cases} \mathcal{A}_1^\mu = -\frac{i}{p} \hat{P}^\mu \not{p}_T \Lambda^+ \\ \mathcal{A}_2^\mu = \hat{P}^\mu \Lambda^+ \\ \mathcal{A}_3^\mu = \hat{p}_T^\mu \not{p}_T \Lambda^+ \\ \mathcal{A}_4^\mu = \frac{i}{p} p_T^\mu \Lambda^+ \\ \mathcal{A}_5^\mu = \gamma_T^\mu \Lambda^+ - \mathcal{A}_3^\mu \\ \mathcal{A}_6^\mu = \frac{i}{p} \gamma_T^\mu \not{p}_T \Lambda^+ - \mathcal{A}_4^\mu, \end{cases}. \quad (30)$$

Here and in the following, the subscript T denotes contraction with $\delta_{\mu\nu} - \hat{P}_\mu \hat{P}_\nu$ to project 4-vectors onto the subspace transverse to the nucleon momentum, *e.g.*, $p_T = p - \hat{P}(p \cdot \hat{P})$. While the decomposition (30) is well suited for numerical processing, there exists an alternative decomposition of the Faddeev amplitude into components which for a nucleon at rest lead to spin and orbital angular-momentum eigenstates [9]. The uniquely defined amplitudes in this partial wave decomposition are certain linear combinations of the functions S_i and A_i as defined by eqs. (27,30) above.

Since the constraints on the vertex function apply in the same way also to the quark-diquark Bethe-Salpeter wave function Ψ defined in eq. (20), its

analogous decomposition reads,

$$\begin{pmatrix} \Psi^5(p, P) \\ \Psi^\mu(p, P) \end{pmatrix} = \begin{pmatrix} \sum_{i=1}^2 \hat{S}_i(p^2, \hat{p} \cdot \hat{P}) \mathcal{S}_i(p, P) \\ \sum_{i=1}^6 \hat{A}_i(p^2, \hat{p} \cdot \hat{P}) \gamma_5 \mathcal{A}_i^\mu(p, P) \end{pmatrix}. \quad (31)$$

The coefficient functions \hat{S}_i , \hat{A}_i herein can be expressed in terms of the S_i , A_i that occur in the decomposition (27) of the vertex function Φ . The explicit expressions follow readily from the relation $\Psi = G_0 \circ \Phi$, *c.f.*, eqs. (20,22).

With the formalism being fully Poincaré covariant we are free to choose the Lorentz frame that best suits our purpose of solving the Bethe–Salpeter equations (19-21). As a particularly convenient choice we adopted the nucleon rest frame for the calculations presented herein, with the total and relative momenta, P and p , as given in eqs. (28) and (29), respectively.

The Bethe–Salpeter equations (19-21) are rewritten in terms of equations for the scalar functions S_1, \dots, A_6 . Their numerical solution described in the following section can be divided into two major steps:

- Chebychev expansion of these scalar functions to account for their $\hat{p} \cdot \hat{P}$ dependences and Chebyshev polynomial approximation of the product of the free quark and diquark propagators in the variable $\hat{p} \cdot \hat{P}$ and of the quark exchange kernel in the two variables $\hat{p} \cdot \hat{P}$ and $\hat{k} \cdot \hat{P}$.
- Solution by numerical iteration of the coupled system of one-dimensional integral equations resulting for the Chebychev moments of the scalar functions.

Note that the expansion in terms of Chebychev polynomials employed in step two, though similar in nature, is not quite the same as a hyperspherical expansion. The Chebychev expansion turns out to be extremely efficient here. Since typically only a few Chebychev polynomials are needed, see below, the numerical effort is greatly reduced as compared to any attempt at calculating the amplitude and the wave function directly on a two-dimensional grid.

The underlying reason for this efficiency relates to the symmetries of Bethe–Salpeter equations in certain limits. For a more detailed discussion of the analogous method within the Wick–Cutkosky model see, *e.g.*, section one of ref. [17] and the references therein. The numerical solution of the ladder-approximate Bethe–Salpeter equation in the massless as well as the massive Wick–Cutkosky model has been studied extensively in the literature, for a review see [18] and for a detailed numerical investigation see ref. [19]. This model describes the interactions of massive scalar particles by a likewise scalar but possibly massless particle exchange. In the case of a massless exchange-particle, the Bethe–Salpeter equation exhibits an $O(4)$ symmetry [20]. By

expanding the wave functions into hyperspherical harmonics one finds that the zero orbital angular momentum states of the Wick–Cutkosky model are essentially given by Chebyshev polynomials of the *second* kind $U_n(z)$. These are related to the Chebyshev polynomials of the *first* kind $T_n(z)$, used in our expansions below, by [21]

$$T_n(z) = U_n(z) - zU_{n-1}(z), \quad (n > 0). \quad (32)$$

This thus exemplifies the close relation between the expansions of wave functions in terms of the T_n 's and those into hyperspherical harmonics.

The quark-diquark Bethe–Salpeter equations (19-21), as derived from the relativistic Faddeev equations under the separable assumption, result to be of a ladder-exchange type also. Here, the mixing of different angular momentum components leads to additional structures, however. This is due to the spinor nature of the Bethe–Salpeter wave function. Much the same as for ordinary Dirac spinors, its lower components have different angular momentum than the upper ones in the relativistic treatment of a spin- $\frac{1}{2}$ bound state. In order to obtain a closed system of equations, different partial waves have to be taken into account. The expansion into *spinor* hyperspherical harmonics is nevertheless possible and it convergences rapidly due to an approximate $O(4)$ symmetry for fermion-boson Bethe–Salpeter equations of the kind under consideration [14,15]. It is therefore understandable also for physical reasons that the expansion in terms of Chebychev polynomials provides such an efficient numerical technique.

To conclude this section, we discuss the kinematics which can be employed to test the procedure and its limitations. In principle, the eigenvalue $\lambda = 1/g_s^2$ should be independent of the Mandelstam parameter η (see the discussion after eq. (21)). Due to singularities in the propagators, however, without considerable modifications to the numerical procedure, it is not possible to use the whole interval $[0,1]$ for such a test [9,14,15]. Rather, the range allowed for the momentum partitioning parameter η in the nucleon Bethe–Salpeter equation is restricted to

$$\eta \in [1 - m_{sc}/M_n, m_q/M_n], \quad (33)$$

if $m_{ax} \geq m_{sc} > m_q$ is assumed. Singularities in the exchange quark propagator and the diquark vertices employing n -pole scalar functions V , see eq. (14), lead to the additional bounds

$$\eta \in \left[\frac{1}{2}(1 - m_q/M_n), \frac{1}{2}(1 + m_q/M_n) \right], \quad (34)$$

$$\eta \in \left[\frac{1}{3}(1 - 2\lambda_n/M_n), \frac{1}{3}(1 + 2\lambda_n/M_n) \right]. \quad (35)$$

Note that these bounds on the value of η arise in the practical calculations

when performed as outlined above. Though an arbitrary η in $[0,1]$ could be chosen in principle, additional residue terms have to be included beyond these bounds in the Euclidean formulation to account for its proper connection with the underlying Bethe–Salpeter equation in Minkowski space.

Well within the above bounds on the momentum routing, however, pronounced plateaus can be observed in order to verify the η -independence of physical observables [9,14]. The extension of these plateaus increases with increasing orders in the Chebyshev expansions.

As the values of η approach the boundaries given in eqs. (33–35), however, strong variations occur due to the vicinity of the poles in the propagators with the effect that the convergence of their Chebyshev expansion, *c.f.*, eq. (47) below, is slowed down considerably. In order to achieve some sufficient accuracy on the vertex function, larger and larger numbers of Chebyshev moments n_{\max} are then needed to approximate the components of the wave function ψ . The slower convergence of the wave function expansion under these circumstances is also observed in the numerical solutions [9,14,15].

2 Numerical method

2.1 Projection on scalar functions in nucleon rest frame

In the nucleon rest frame (28,29) we express the Euclidean components of p^μ and k^μ (the latter being the integration variable) in hyperspherical coordinates:

$$\begin{pmatrix} k^1 \\ k^2 \\ k^3 \\ k^4 \end{pmatrix} = |k| \begin{pmatrix} \sin \psi' \sin \theta' \sin \phi' \\ \sin \psi' \sin \theta' \cos \phi' \\ \sin \psi' \cos \theta' \\ \cos \psi' \end{pmatrix}, \quad \begin{pmatrix} p^1 \\ p^2 \\ p^3 \\ p^4 \end{pmatrix} = |p| \begin{pmatrix} 0 \\ 0 \\ \sin \psi \\ \cos \psi \end{pmatrix}. \quad (36)$$

To simplify the notation, we set $z = \cos \psi$, $z' = \cos \psi'$. In the chosen frame the vertex function decomposition on the l.h.s of eq. (19) simplifies to

$$\begin{pmatrix} \Phi^5 \\ \Phi^4 \\ \Phi^3 \\ \Phi^2 \\ \Phi^1 \end{pmatrix} (p^2, z) = \begin{pmatrix} \begin{pmatrix} S_1(p^2, z) & 0 \\ \sigma_3 \sqrt{1-z^2} S_2(p^2, z) & 0 \end{pmatrix} \\ \begin{pmatrix} \sigma_3 \sqrt{1-z^2} A_1(p^2, z) & 0 \\ A_2(p^2, z) & 0 \end{pmatrix} \\ \begin{pmatrix} i\sigma_3 A_3(p^2, z) & 0 \\ i\sqrt{1-z^2} A_4(p^2, z) & 0 \end{pmatrix} \\ \begin{pmatrix} i\sigma_2 A_5(p^2, z) & 0 \\ -\sigma_1 \sqrt{1-z^2} A_6(p^2, z) & 0 \end{pmatrix} \\ \begin{pmatrix} i\sigma_1 A_5(p^2, z) & 0 \\ \sigma_2 \sqrt{1-z^2} A_6(p^2, z) & 0 \end{pmatrix} \end{pmatrix}. \quad (37)$$

By virtue of the positive-energy condition and our choice for the covariants in eqs. (30) the vertex (and likewise the wave function) consists of 2×2 -blocks in Dirac space which define upper and lower components for the scalar and Lorentz components of Φ , respectively. The unknown scalar functions do not couple within these blocks. Since we have chosen the most general decomposition, the equations for the Lorentz components Φ^2 and Φ^1 are degenerate.

For convenience we will use generic functions Y_i ($i = 1, \dots, 8$) related to the functions S_i and A_i ,

$$S_{1,2} \rightarrow Y_{1,2}, \quad A_{1\dots 6} \rightarrow Y_{3\dots 8}. \quad (38)$$

The functions \hat{Y}_i substituting the functions \hat{S}_i, \hat{A}_i appearing in the wave function (31) are defined analogously.

Projection onto the scalar functions Y_i and \hat{Y}_i is now done by inspecting the upper and lower components in the equations (20,19) for each Lorentz component. As explained before, the Y_i and \hat{Y}_i neatly decouple in upper and lower components. We arrive at:

$$\hat{Y}_i(p^2, z) = (g'_0)^{ij}(p^2, z) Y_j(p^2, z), \quad (39)$$

$$Y_i(p^2, z) = \int \frac{d^4 k}{(2\pi)^4} (H')^{ij}(p^2, k^2, y', z, z') \hat{Y}_i(k^2, z'). \quad (40)$$

As a result, we obtain the propagator matrix $(g'_0)^{ij}$ and the modified quark exchange kernel matrix $(H')^{ij}$. The latter depends on the possible scalar prod-

ucts between the vectors k, p, P . These scalar products can be expressed as $k^2, p^2, z' = \hat{k} \cdot \hat{P}$, $z = \hat{p} \cdot \hat{P}$ and $y' = \hat{k} \cdot \hat{p}$. We refrain from stating explicitly the lengthy expressions for the quantities $(g'_0)^{ij}$ and $(H')^{ij}$ here.

2.2 Chebyshev Approximation

The approximation of a function by Chebyshev polynomials of the first kind $T_n(z)$ is discussed in detail in ref. [22]. We briefly summarize the necessary formulae. Employing a convenient (albeit non-standard) normalization $T_0 = 1/\sqrt{2}$, the orthogonality relation reads,

$$\int_{-1}^1 \frac{T_n(z)T_m(z)}{\sqrt{1-z^2}} dz = \frac{\pi}{2} \delta_{nm} , \quad (41)$$

Let $\{z_k, k = 1 \dots K\}$ denote the zeros of T_K . The discrete orthogonality relation is

$$\frac{2}{K} \sum_{k=1}^K T_m(z_k)T_n(z_k) = \delta_{mn} . \quad (42)$$

We approximate a function $F(p^2, p \cdot P)$ by a finite sum of T 's in the variable $z = \hat{p} \cdot \hat{P}$:

$$F(p^2, p \cdot P) = \sum_{n=0}^{n_{\max}} i^n F^n(p^2) T_n(z) , \quad (43)$$

$$F^n(p^2) = (-i)^n \sum_{k=1}^{n_{\max}+1} T_n(z_k) F(p^2, z_k) . \quad (44)$$

As before, the $\{z_k\}$ are the zeros of $T_{n_{\max}+1}$. Note that for a finite n_{\max} the such defined Chebyshev moments $F^n(p^2)$ are *not* identical to the projections of eq. (43) using eq. (41), rather eqs. (43,44) are very close to the approximation of F by the *minimax polynomial*, which (among all polynomials of the same degree) has the smallest maximum deviation from the true function [22]. For $z = z_k$ and/or $n_{\max} \rightarrow \infty$, projection and approximation are of course identical, courtesy of eq. (42).

We use this method to approximate propagators and the exchange kernel in eqs. (39,40). Expanding the amplitudes of wave and vertex function as

$$Y_i(p^2, z) = \sum_{m=0}^{m_{\max}} i^m Y_i^m(p^2) T_m(z), \quad (45)$$

$$\hat{Y}_i(p^2, z) = \sum_{n=0}^{n_{\max}} i^n \hat{Y}_i^n(p^2) T_n(z), \quad (46)$$

and applying eqs. (43,44) to $(g'_0)^{ij}$ in eq. (39), we obtain the matrix equation

$$\hat{Y}_i^n(p^2) = (g_0)^{ij, nm}(p^2) Y_j^m(p^2), \quad (47)$$

$$(g_0)^{ij, nm}(p^2) = \frac{2}{p_{\max} + 1} \sum_{k=1}^{p_{\max}} (g'_0)^{ij}(p^2, z_k) i^{j-i} T_n(z_k) T_m(z_k). \quad (48)$$

The projection onto the Y_i^n was done using the orthogonality relation (41). In practice, we choose $p_{\max} = n_{\max} + m_{\max}$ for a reliable approximation of the propagator matrix. The elements of the propagator matrix $(g_0)^{ij, nm}$ are all real due to the explicit phase factor i^n in the Chebyshev expansions (45,46).

The Chebyshev approximation in the variables z and z' is now applied to the matrix $(H')^{ij}$ in eq. (40):

$$(H'')^{ij} = (1 - z'^2)(H')^{ij} = \sum_{s=1}^{m_{\max}+1} \sum_{t=1}^{n_{\max}+1} c^{ij, st} T_{s-1}(z) T_{t-1}(z'). \quad (49)$$

$$c^{ij, st} = \frac{2}{(m_{\max} + 1)} \frac{2}{(n_{\max} + 1)} \sum_{u=1}^{m_{\max}+1} \sum_{v=1}^{n_{\max}+1} T_{s-1}(z_u) T_{t-1}(z'_v) \times (H'')^{ij}(p^2, k^2, y', z_u, z'_v). \quad (50)$$

The $\{z_u\}$ and $\{z'_v\}$ are the zeros of the Chebyshev polynomial $T_{m_{\max}+1}(z)$ and $T_{n_{\max}+1}(z')$, respectively. We insert this expression into eq. (40), as well as the expansions (45,46) for wave and vertex function. After projecting onto the Y_i^m the integrations over z and z' on the r.h.s. are done using the orthogonality relation (41) and we obtain:

$$Y_i^m(p^2) = \frac{1}{(m_{\max} + 1)(n_{\max} + 1)} \int_0^\infty \frac{k^3}{4\pi^2} d|k| \int_{-1}^1 dy' \sum_{u=1}^{m_{\max}+1} \sum_{v=1}^{n_{\max}+1} i^{n-m} \times T_m(z_u) T_n(z'_v) (H'')^{ij}(p^2, k^2, y', z_u, z'_v) \hat{Y}_j^n(k^2). \quad (51)$$

Here the sum runs also over the label j and the Chebyshev moment label n .

We have now succeeded to transform the original 4-dimensional integral equation into a system of coupled one-dimensional equations. In summary, the system reads,

$$\hat{Y}_i^n(p^2) = (g_0)^{ij, nm}(p^2) Y_j^m(p^2), \quad (52)$$

$$Y_i^m(p^2) = \int_0^\infty d|k| H^{ij, mn}(k^2, p^2) \hat{Y}_j^n(k^2), \quad (53)$$

where indices appearing twice are summed over. Furthermore, the definition

$$H^{ij, mn}(k^2, p^2) = \frac{1}{(m_{\max} + 1)(n_{\max} + 1)} \frac{k^3}{4\pi^2} \int_{-1}^1 dy' \sum_{u=1}^{m_{\max}+1} \sum_{v=1}^{n_{\max}+1} i^{n-m} \\ \times T_m(z_u) T_n(z'_v) (H'')^{ij}(p^2, k^2, y', z_u, z'_v) \quad (54)$$

is used.

2.3 Solving the coupled one-dimensional integral equations

The integration variable in eq. (53) is the absolute value of the four momentum k . It will be discretized on a mesh with $n_{|k|}$ points, with typically $n_{|k|} = 20, \dots, 50$, and the integration is performed as a Gaussian quadrature. In the actual version of the program, the integration domain is first mapped onto the interval $[-1, 1]$ with the help of the transformation $x = (|k| - 1)/(|k| + 1)$ and then a Gauss–Legendre integration is used.

After this step, the problem has become equivalent to finding the largest eigenvalue of a matrix equation. To this end we employ an iterative method: Some initial values for the vertex functions, *i.e.* for the moments Y_i^m , are chosen, and eq. (52) is used to calculate the corresponding expression for the wave function, *i.e.* for the moments \hat{Y}_i^n . Eq. (53) provides the moments Y_i^m in the next iteration step. If $Y_1^0(p^2)$ deviates more than a given accuracy (provided in the input file) for some momentum on the grid the updated moment $Y_1^0(p^2)$ at the grid point with the largest deviation is used to update the coupling constant g_s . This value and renormalized functions Y_i^m are then the starting point for the next iteration step. Requiring an accuracy of the order 10^{-9} convergence is usually reached after 20 - 30 iteration steps.

The correct nucleon mass corresponds to the eigenvalue $\lambda = 1/g_s^2$. To determine it, in a first step eigenvalues $\lambda(M_1)$ and $\lambda(M_2)$ are calculated with $M_1 = \max[m_q, m_{sc}, m_{ax}]$ and $M_2 = \min[m_q/\eta, m_{sc}/(1-\eta), m_{ax}/(1-\eta)]$. These starting values are motivated by the observation that for physically reasonable parameters the nucleon mass should be larger than the quark and diquark masses, and, for a given choice of η , M_2 represents the upper limit beyond which singularities are encountered in the quark and diquark propagators. Now the nucleon mass M for which $\lambda(M) = 1/g_s^2$ holds is determined by linear bisection in the next step and by quadratic interpolation in all following

Set	η	m_q [GeV]	m_{sc} [GeV]	m_{ax} [GeV]	c_0 [GeV]	g_s	g_a	M [GeV]
I	0.36	0.360	0.6255	0.6840	0.95	9.29	6.97	0.939
II	0.40	0.425	0.5977	0.8314	0.53	22.10	6.37	0.939

Table 1

The two parameter sets together with the values of couplings and the bound mass M that arise for these sets. The maximal number of Chebyshev polynomials for vertex and wave function is given by $m_{\max} = 8$ and $n_{\max} = 12$ and the number of momentum grid points is $n_{|k|} = 40$. The y' integration was done using Gaussian quadrature with $n_y = 32$ grid points.

steps. Typically 5 - 8 steps are needed to arrive at an accuracy of the order of 10^{-5} . During each step the integral equation has to be solved anew for its largest eigenvalue, thus illustrating the need for a fast algorithm which is provided here.

As the system under consideration is a linear integral equation, the normalization for the functions Y_i^m and \hat{Y}_i^n stays undetermined. Without loss of generality we fix the value of the lowest Chebychev moment of the first upper component of the vertex function at the smallest absolute value on the momentum grid,

$$Y_1^0(p_{\min}^2 \approx 0) = 1, \quad (55)$$

and renormalize accordingly all functions Y_i^m and \hat{Y}_i^n in the output routine. These vertex and wave functions are then the final result of the algorithm.

3 Numerical Results

To keep this article reasonably self-contained we will present numerical results only for two example sets of parameters. Quite a number of results obtained with this program can be found in refs. [9,13–15]. Altogether there are four parameters: the quark mass m_q , the diquark masses m_{sc} and m_{ax} , and the width c_0 of the dipole-shaped diquark-quark vertex (14). Diquark masses and the width determine the coupling constants g_a and g_s . Note that in actual applications g_a and therefore m_{ax} is determined by fitting the mass of the Δ baryon, see *e.g.* ref. [9] for more details. The equation for the Δ baryon is solved by an algorithm completely analogous to the one presented here. The results for two characteristic parameter sets are given in table 1.

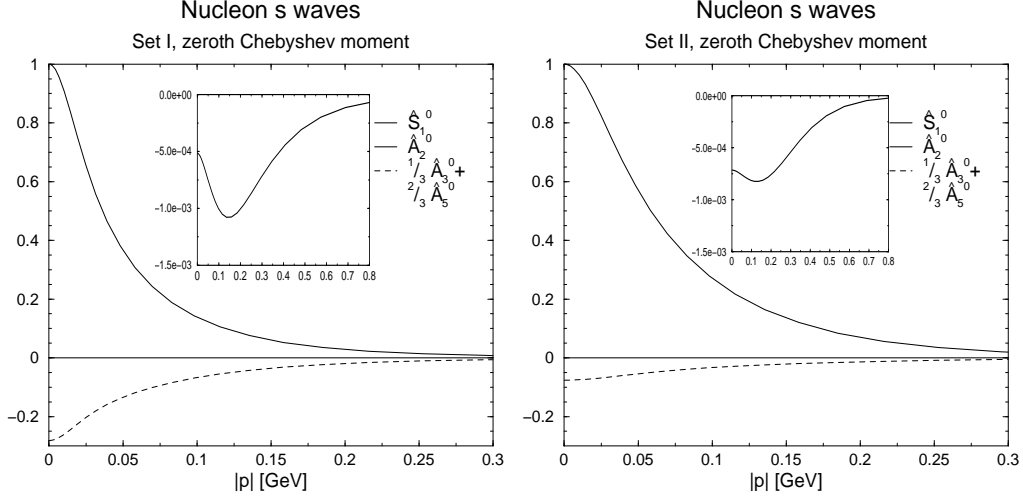


Fig. 2. The leading Chebyshev moments of the functions \hat{S}_1 , \hat{A}_2 and $(1/3)\hat{A}_3 + (2/3)\hat{A}_5$ related to the nucleon s waves. All functions are normalized by the condition $\hat{S}_1^0 = 1$.

Although the wave and the vertex function are no physical observables they do enter observable matrix elements (see *e.g.* refs. [13–15]) and therefore the strengths of the single components give a hint on their effect on observables. We have plotted the leading Chebyshev moments of the scalar functions describing the nucleon s waves in figure 2. These are \hat{S}_1^0 and $(1/3)\hat{A}_3^0 + (2/3)\hat{A}_5^0$, describing the s waves for scalar and axialvector diquark and \hat{A}_2^0 that is connected with the virtual time component of the latter. We see for both sets that the functions \hat{A}_2^0 are suppressed by a factor of 10^3 compared to the dominating \hat{S}_1^0 . The strength of the other s wave associated with the axialvector diquark is roughly proportional to the ratio g_a/g_s for the respective parameter set.

In figure 3 we have plotted the 0^{th} , 2^{nd} and 4^{th} Chebychev moments (the odd ones have been left out for clarity of the presentation) of the linear combinations of the functions \hat{S}_i and \hat{A}_i which belong to the eigenfunctions to the (3 quark) spin operator and the operator of angular momentum between quark and diquark [15]. One sees easily that in the nucleon rest frame higher Chebychev moments become unimportant very fast.

4 Summary and Applications

In summary, we have succeeded in developing an efficient algorithm for the calculation of the nucleon amplitudes in the seperable approximation to the Poincaré covariant three-quark Faddeev equation. To this end we employ an approximate $O(4)$ symmetry of the resulting effective diquark-quark Bethe–Salpeter equation by using a Chebychev expansion. This allows to transform

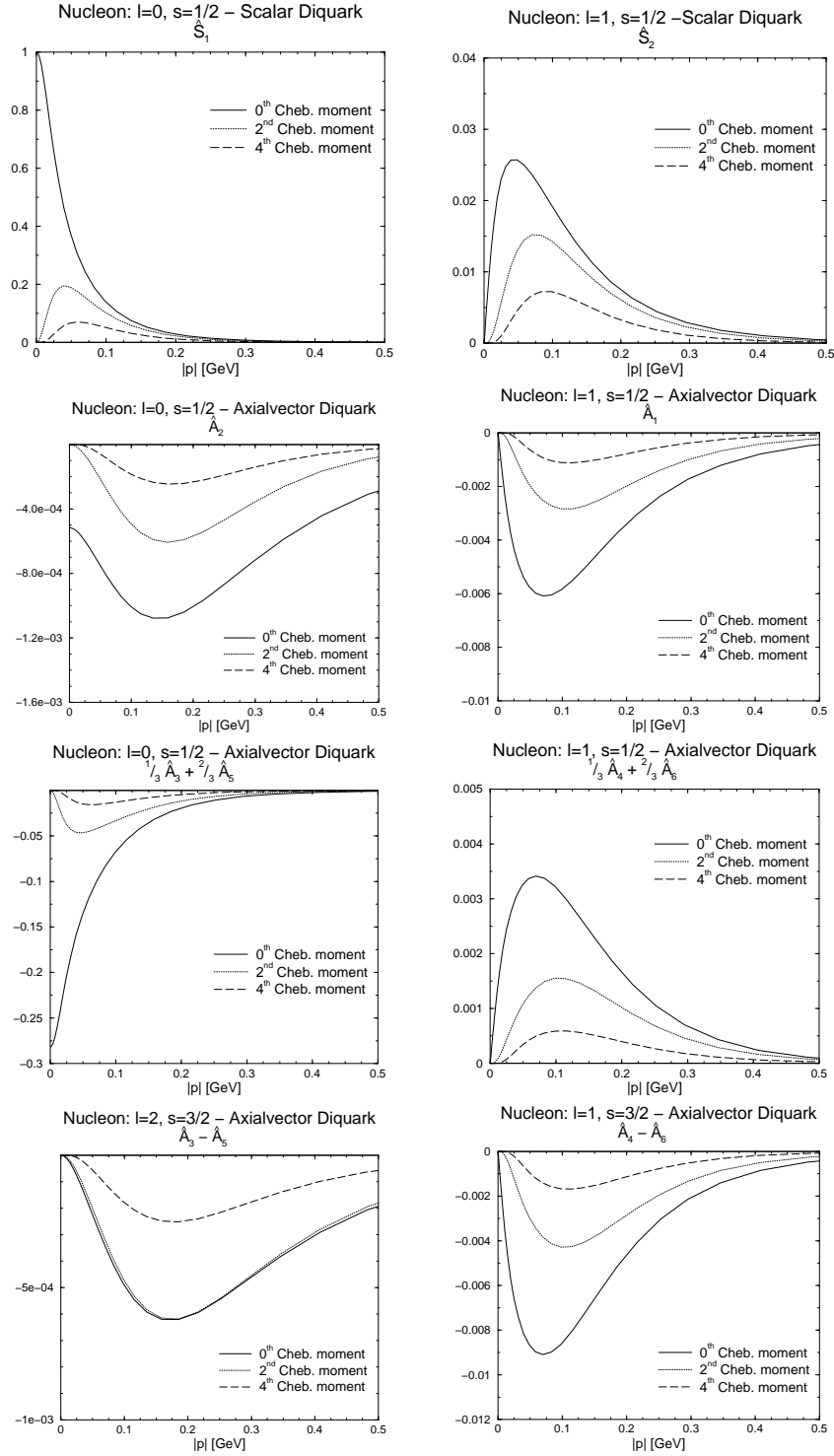


Fig. 3. Chebyshev moments of the scalar functions describing the strengths of quark–diquark partial waves with quantum number s for the total quark–diquark spin and quantum number l for the orbital angular momentum.

the full 4-dimensional problem into a manageable form.

The chosen expansion in Dirac space into partial waves has been done covariantly and the results for the partial wave strengths identify the leading and subleading components. The Chebyshev expansion for the scalar functions which describe the partial wave strengths has proved to be quite efficient and accurate, furthermore the expansion has been done for a Lorentz invariant variable, with the consequence that the boost of the wave and vertex function solutions is rendered feasible.

The latter point is of utter importance because the applications of the presented results to calculate physical observables require to Lorentz boost the Bethe–Salpeter wave function. Please note also that in Lorentz frames where the nucleon is moving higher Chebychev moments will become increasingly important with increasing nucleon momentum. Nevertheless, based on the presented algorithm nucleon form factors have been calculated up to several GeV of transferred momentum [14], and even production processes have been studied for a similar energy range [13].

Given the fact that the required CPU time to run this program is very moderate even on PCs, and that the underlying Poincaré invariant nucleon model has a much broader application range than non-relativistic models we are confident that the presented model and the related algorithm will find wide-spread use in future investigations of nucleon properties.

5 Description of the Program

5.1 *The main program*

Before the main program we have included a **module global** to provide a global definition of the input parameters. Furthermore, the integration points and weights are defined globally.

The main program calls the subroutine **read_parameters**, allocates memory space for the used fields, and calls then the subroutine **int_weights** three times determining thereby the integration points and weights for the one angle and the one momentum integration. Note that the momenta $pp \in [0, \infty]$ are mapped to the interval $[0,1]$ for a Gauss–Legendre quadrature of the momentum integration.

The subroutine **dqnorms** is called to calculate g_s and g_a as prescribed by eqs. (16,17).

Then the iteration loop for the nucleon mass is started with two initial values for the bound state mass M . During each iteration step the main algorithm, given in the subroutine **bsemain** is called which calculates the vertex function, the wave function and the coupling $g_s = 1/\sqrt{\lambda}$ which corresponds to the mass M . The mass is updated by bisection until satisfactory agreement between $1/\sqrt{\lambda}$ and the scalar diquark normalization is reached.

Calling the subroutine **output** concludes the main program.

5.2 *Input and Output*

Reading the input and writing out the vertex function, the wave function and the coupling g_s is deferred to the subroutines **read_parameters** and **output**. The format in which the parameters are read in and the results are written out is obvious from the appended sample input and sample output.

5.3 *The subroutines “bsemain” and “bse_kernel”*

The first action to be taken in the subroutine **bsemain** is to call the subroutine **bse_kernel** to generate the kernel of the equation as given in eq. (54). This includes the integration over y' and the summation over the zeros of the Chebychev polynomials. A complex auxiliary array s is introduced whose real part, denoted r , is then used to provide the explicit expression for the kernel.

Next, the propagator matrix $(g_0)^{ij,mn}$ is generated, via the intermediary steps of specifying the numerator of the matrix $(g'_0)^{ij}$ and the application of eq. (48).

Then the Chebychev moments Y_i^m are initialized, all by the same function pe^{-p} . The iteration is implemented by a DO WHILE loop. In the iteration loop, first the Chebychev expansion of the propagators (denominators and numerators) and in a subsequent step the one of the product of quark and diquark propagators is determined. This allows to calculate the functions \hat{Y}_i^n , *i.e.* the wave function Ψ , from eq. (20). Finally, eq. (19) with the calculated kernel is used to update the vertex function Φ (the Y_i^m). The new function Y_1^0 is used as described in sect. 3 to update g_s and to test for convergence.

5.4 *Further Subroutines and Functions*

The subroutine **int_weights** calculates the integration points and weights for Gauss–Legendre quadrature.

n_{\max}	2	4	6	8	10	12
m_{\max}						
0	0.8910	0.9156	0.9212	0.9225	0.9228	0.9229
2	0.9193	0.9321	0.9352	0.9360	0.9362	0.9363
4		0.9365	0.9381	0.9386	0.9387	0.9388
6			0.9387	0.9389	0.9390	0.9390
8				0.9390	0.9390	0.9390

Table 2

Convergence of the bound state mass M [GeV] in terms of m_{\max} and n_{\max} . Due to weaker convergence of the wave function, only $n_{\max} > m_{\max}$ is considered. For momentum and angular integration $n_{|k|} = n_y = 20$ grid points have been used.

The RECURSIVE FUNCTION **Chebyone** determines the values of the Chebyshev polynomials of the first kind.

The FUNCTION **dq** implements the diquark function (14).

6 Testing the program

Of course, trivial tests establishing the independence of the number of integration points etc. have been performed. We also verified that the vertex and wave functions are independent of the initializing functions.

In table 2 we demonstrate the convergence of the bound state mass in terms of m_{\max} and n_{\max} . We have chosen parameter set I from table 1 for that purpose. Since in the scalar diquark channel the binding energy is just 46 MeV, one might not expect good convergence due to the nearby poles in quark and diquark propagators. Nevertheless, already for $m_{\max} = 6$ and $n_{\max} = 8$ the nucleon mass is exact up to 0.1 MeV.

A very non-trivial test consists in changing the Mandelstam parameter η , see the discussion the end of sect. 1. Please note that changing η may necessitate an increase in the order of the Chebyshev expansion in order to obtain comparable accuracy.

Acknowledgements

We are grateful to Steven Ahlig, Christian Fischer, Gerhard Hellstern, Mike Pichowsky, Hugo Reinhardt, Craig Roberts, Sebastian Schmidt and Herbert Weigel for their collaboration on related issues in this model and helpful discussions.

We thank Sebastian Schmidt for a critical reading of this manuscript.

The work reported here has been supported by a Feodor-Lynen fellowship of the Alexander-von-Humboldt foundation for M.O. and by COSY under contract no. 4137660.

R.A. and L.v.S. want to express their gratitude to the members of the CSSM, University of Adelaide, for the hospitality experienced during their visits.

References

- [1] I. R. Afnan and A. W. Thomas, “Fundamentals Of Three Body Scattering Theory,” In **Topics In Current Physics, Vol.2**, Berlin 1977, 1-47
- [2] R. T. Cahill, C. D. Roberts and J. Praschifka, Austral. J. Phys. **42** (1989) 129.
- [3] H. Reinhardt, Phys. Lett. **B244** (1990) 316.
- [4] A. Buck, R. Alkofer and H. Reinhardt, Phys. Lett. B **286** (1992) 29.
- [5] N. Ishii, W. Bentz and K. Yazaki, Nucl. Phys. **A587** (1995) 617.
- [6] U. Zückert, R. Alkofer, H. Weigel and H. Reinhardt, Phys. Rev. **C55** (1997) 2030 [nucl-th/9609012].
- [7] A. Bender, C. D. Roberts and L. von Smekal, Phys. Lett. **B380** (1996) 7 [nucl-th/9602012].
- [8] G. Hellstern, R. Alkofer and H. Reinhardt, Nucl. Phys. **A625** (1997) 697 [hep-ph/9706551].
- [9] M. Oettel, “Baryons as Relativistic Bound States of Quark and Diquark,” Ph. D. Thesis, Tübingen University, 2000, <http://w210.ub.uni-tuebingen.de/dbt/volltexte/2000/177> [nucl-th/0012067].
- [10] R. Alkofer and M. Oettel, “Nucleon form factors in the covariant diquark-quark model,” Proceedings of the Workshop on ”Lepton scattering, Hadrons and QCD”, Adelaide, March 26 to April 6, 2001 [hep-ph/0105320].
- [11] R. Alkofer and L. von Smekal, Physics Reports **353** (2001) 281 [hep-ph/0007355].
- [12] C. D. Roberts and S. M. Schmidt, Prog. Part. Nucl. Phys. **45** (2000) S1 [nucl-th/0005064].

- [13] S. Ahlig, R. Alkofer, C. Fischer, M. Oettel, H. Reinhardt and H. Weigel, Phys. Rev. **D64** (2001) 014004. [hep-ph/0012282].
- [14] M. Oettel, M. Pichowsky and L. von Smekal, Eur. Phys. J. **A8** (2000) 251 [nucl-th/9909082]; M. Oettel, R. Alkofer and L. von Smekal, Eur. Phys. J. **A8** (2000) 553 [nucl-th/0006082]; M. Oettel and R. Alkofer, Phys. Lett. **B484** (2000) 243 [hep-ph/0001261].
- [15] G. Hellstern, R. Alkofer, M. Oettel and H. Reinhardt, Nucl. Phys. **A627** (1997) 679 [hep-ph/9705267]; M. Oettel, G. Hellstern, R. Alkofer and H. Reinhardt, Phys. Rev. **C58** (1998) 2459 [nucl-th/9805054].
- [16] J. C. Bloch, C. D. Roberts and S. M. Schmidt, Phys. Rev. **C61** (2000) 065207 [nucl-th/9911068]; J. C. Bloch, C. D. Roberts, S. M. Schmidt, A. Bender and M. R. Frank, Phys. Rev. **C60** (1999) 062201 [nucl-th/9907120].
- [17] S. Ahlig and R. Alkofer, Annals Phys. **275** (1999) 113 [hep-th/9810241].
- [18] N. Nakanishi, Prog. Theor. Phys. Suppl. **95** (1988) 1.
- [19] T. Nieuwenhuis and J. A. Tjon, Few Body Syst. **21** (1996) 167 [nucl-th/9607041].
- [20] R. E. Cutkosky, Phys. Rev. **96** (1954) 1135.
- [21] M. Abramowitz and I. A. Stegun, *Handbook of Mathematical Functions*, Dover, New York, USA, 1965.
- [22] W. H. Press, B. P. Flannery, S. A. Teukolsky, and W. T. Vetterling, *Numerical Recipes (FORTRAN Version)*, Cambridge University Press, Cambridge, UK, 1989.

TEST RUN

input file:

```
quark mass : 0.36
scalar diquark mass : 0.6255
axialvector diquark mass : 0.684
diquark width : 0.95
type of diquark amplitude : 1
exponent of diquark amplitude : 2
momentum partitioning eta : 0.36
npe - momentum grid |k|,|p| : 20
ny - angle grid \vec k \cdot \vec p : 20
mmax - Chebyshev accuracy VF : 6
nmax - Chebyshev accuracy WF : 8
accuracy for eigenvalue : 1.D-9
accuracy for mass : 1.D-5
output file : sa.out
```

standard output:

```
gs : 9.289520 ga : 6.965978

mass iteration # 1
M_N = 0.684000
calculating H_kernel...
generated VF Chebyshev moments
0 1 2 3 4 5 6 H_kernel done!
# it 1/sqrt(lambda)
5 0.15781675145113D+02
10 0.16128853436214D+02
15 0.16125685785706D+02
20 0.16125712415957D+02
25 0.16125712185873D+02
25 0.16125712185873D+02
|gs-1/sqrt(lambda)| / gs: 0.735904

mass iteration # 2
M_N = 0.976984
calculating H_kernel...
generated VF Chebyshev moments
0 1 2 3 4 5 6 H_kernel done!
# it 1/sqrt(lambda)
5 0.66709436074472D+01
10 0.71005125223069D+01
15 0.70958216340534D+01
20 0.70958710453183D+01
25 0.70958705246610D+01
27 0.70958705292115D+01
|gs-1/sqrt(lambda)| / gs: 0.236142

mass iteration # 3
M_N = 0.905808
calculating H_kernel...
generated VF Chebyshev moments
0 1 2 3 4 5 6 H_kernel done!
# it 1/sqrt(lambda)
```

```
5 0.99728969409881D+01
10 0.10508348360659D+02
15 0.10500476420175D+02
20 0.10500595152654D+02
25 0.10500593361326D+02
29 0.10500593387021D+02
|gs-1/sqrt(lambda)| / gs: 0.130370
```

```
mass iteration # 4
M_N = 0.936576
calculating H_kernel...
generated VF Chebyshev moments
0 1 2 3 4 5 6 H_kernel done!
# it 1/sqrt(lambda)
5 0.88748406217450D+01
10 0.93909382462111D+01
15 0.93830314492941D+01
20 0.93831520978449D+01
25 0.93831502564257D+01
29 0.93831502831329D+01
|gs-1/sqrt(lambda)| / gs: 0.010079
```

```
mass iteration # 5
M_N = 0.938826
calculating H_kernel...
generated VF Chebyshev moments
0 1 2 3 4 5 6 H_kernel done!
# it 1/sqrt(lambda)
5 0.87863777879217D+01
10 0.93005927655577D+01
15 0.92927115567109D+01
20 0.92928316413400D+01
25 0.92928298111699D+01
29 0.92928298376773D+01
|gs-1/sqrt(lambda)| / gs: 0.000356
```

```
mass iteration # 6
M_N = 0.938908
calculating H_kernel...
generated VF Chebyshev moments
0 1 2 3 4 5 6 H_kernel done!
# it 1/sqrt(lambda)
5 0.87831354990374D+01
10 0.92972802606202D+01
15 0.92894000862408D+01
20 0.92895201477319D+01
25 0.92895183180267D+01
29 0.92895183445258D+01
|gs-1/sqrt(lambda)| / gs: 0.000000
```

done...

output file:

```
#####
# mq      : 0.360000 ms      : 0.625500 ma      : 0.684000
# M       : 0.938908 ga/gs   : 0.749875 gs      : 9.289518
# eta     : 0.360000
```

```

# Dq.ampl. : RATIONAL co      : 0.950000 nexp      :      2
# mmax     :      6 nmax     :      8
# npe      :      20 ny      :      20
#####
# VERTEX FUNCTION
# S_1      |p|      0      1      2      3      4      5      6
0.3448D-02 0.1000D+01 0.1038D-01 0.7696D-04 0.6986D-06 0.7131D-08 0.8341D-10 0.1139D-11
0.1834D-01 0.9948D+00 0.5474D-01 0.2145D-02 0.1029D-03 0.5536D-05 0.3407D-06 0.2456D-07
0.4590D-01 0.9678D+00 0.1305D+00 0.1237D-01 0.1432D-02 0.1842D-03 0.2677D-04 0.4692D-05
0.8748D-01 0.8953D+00 0.2176D+00 0.3596D-01 0.7225D-02 0.1588D-02 0.3804D-03 0.1175D-03
0.1453D+00 0.7662D+00 0.2796D+00 0.6502D-01 0.1845D-01 0.5651D-02 0.1777D-02 0.7879D-03
0.2225D+00 0.5949D+00 0.2891D+00 0.8072D-01 0.2801D-01 0.1042D-01 0.3755D-02 0.2042D-02
0.3237D+00 0.4110D+00 0.2470D+00 0.7298D-01 0.2822D-01 0.1145D-01 0.4387D-02 0.2579D-02
0.4559D+00 0.2447D+00 0.1751D+00 0.4881D-01 0.2015D-01 0.8083D-02 0.3158D-02 0.1822D-02
0.6289D+00 0.1197D+00 0.1011D+00 0.2350D-01 0.1047D-01 0.3758D-02 0.1465D-02 0.7767D-03
0.8578D+00 0.4528D-01 0.4562D-01 0.7580D-02 0.4001D-02 0.1127D-02 0.4489D-03 0.2107D-03
0.1166D+01 0.1244D-01 0.1527D-01 0.1415D-02 0.1123D-02 0.1986D-03 0.9469D-04 0.3774D-04
0.1590D+01 0.2337D-02 0.3555D-02 0.8715D-04 0.2243D-03 0.1414D-04 0.1433D-04 0.4083D-05
0.2193D+01 0.2812D-03 0.5378D-03 -0.1529D-04 0.2902D-04 -0.9603D-06 0.1489D-05 0.1644D-06
0.3089D+01 0.1989D-04 0.4910D-04 -0.2865D-05 0.2078D-05 -0.1842D-06 0.8582D-07 -0.3406D-08
0.4495D+01 0.7375D-06 0.2526D-05 -0.1597D-06 0.6870D-07 -0.6718D-08 0.1966D-08 -0.1851D-09
0.6884D+01 0.1259D-07 0.6794D-07 -0.3476D-08 0.9234D-09 -0.7024D-10 0.1214D-10 -0.8321D-12
0.1143D+02 0.8325D-10 0.7912D-09 -0.2673D-10 0.4159D-11 -0.2141D-12 0.1727D-13 -0.7142D-15
0.2179D+02 0.1342D-12 0.2495D-11 -0.4574D-13 0.3731D-14 -0.9881D-16 -0.1453D-16 -0.1259D-18
0.5451D+02 0.1406D-16 0.6590D-15 -0.4875D-17 0.1569D-18 -0.1834D-20 0.3594D-22 -0.4368D-24
0.2901D+03 0.7739D-24 0.1932D-21 -0.2691D-24 0.1628D-26 -0.3582D-29 0.1522D-31 -0.4176D-34
# S_2      |p|      0      1      2      3      4      5      6
0.3448D-02 -0.2451D-02 -0.1331D-04 -0.1071D-06 -0.8120D-09 -0.5374D-11 -0.6284D-14 0.8165D-15
0.1834D-01 -0.1299D-01 -0.3733D-03 -0.1594D-04 -0.6428D-06 -0.2298D-07 -0.2126D-09 0.8966D-10
0.4590D-01 -0.3185D-01 -0.2217D-02 -0.2331D-03 -0.2338D-04 -0.2208D-05 -0.1132D-06 0.3099D-07

```

...